

as follows. The real differences in row and column are 42 mm, close to our transformed values.

Camera Id	Mean (mm)	Median (mm)	Variance (mm)
0	42.21	42.22	0.12
1	42.05	42.02	0.13
2	42.37	42.37	0.07
3	42.20	42.21	0.13

Table 2: Statistic results of row difference .

Camera Id	Mean (mm)	Median (mm)	Variance (mm)
0	41.97	42.00	0.09
1	41.68	41.69	0.10
2	41.93	41.93	0.07
3	41.55	41.63	0.45

Table 3: Statistic results of column difference .

### 5.3 Dot Based Evaluation

#### Dot Based Evaluation Overview

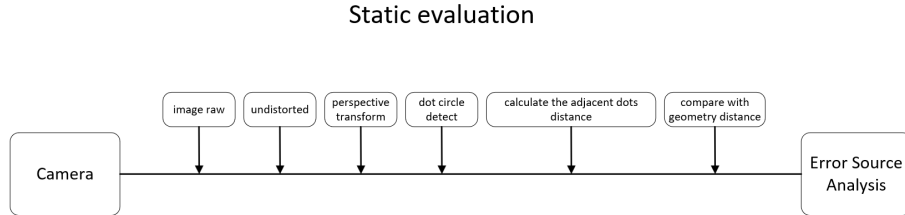


Figure 17: Overview of Dot Based Evaluation in static

Figure 17 illustrates the static evaluation process used to determine the precision of converting pixel distances to real world distances using a dot-based calibration method. The process consists of the following steps:

1. **Camera capture:** The camera captures the raw image that contains the dot pattern. In this project, we use both 2k and 4k resolution images.
2. **Undistorted:** In the laboratory, we have four ceiling-mounted high-definition video cameras, which exhibit some pincushion distortion. Additionally, the camera's autofocus function is disabled during operation to prevent

focus adjustments from affecting the evaluation process. Lens distortion is corrected to produce an undistorted image, ensuring geometric accuracy in subsequent steps.

3. **Perspective Transform:** A perspective transformation is applied to align the image plane, removing any perspective distortions and standardizing the view. To achieve this, we placed 10 AprilTags on the ground with pre-measured relative positions. To ensure that the AprilTags are positioned more accurately at the pre-designed and measured locations, we used cotton strings as reference lines to verify whether the AprilTags were aligned correctly. The camera's relative position is determined by detecting these AprilTags, and a perspective transformation matrix is computed. This matrix is then used to convert the image into a bird's-eye view for subsequent processing. **In this project, we map one pixel in the image into one millimeter in real world.**
4. **Dot Circle Detection:** In this step, image processing techniques such as contour detection are used to identify the circular dots in the image. The center coordinates and the radius of the circles are calculated based on the detected contours. **In this project, the distance between the adjacent dots is 42 millimeter and the radius of the dot is 10 millimeter.**
5. **Calculate the distances of adjacent dots:** Using the center coordinates of the detected circular dots, the Euclidean distances between the centers of adjacent circular dots in the same row or column are calculated. These computed distances in the image are then compared with the actual geometric distances to evaluate accuracy.
6. **Compare with Geometric Distance:** The calculated pixel distances are compared with the known real-world geometric distances between the dots. This comparison provides a measure of accuracy in the pixel-to-real-world distance mapping. **In this project, one pixel in the image corresponding to one millimeter in the real world.**
7. **Error Source Analysis:** To evaluate the accuracy of the pixel-distance mapping system, we conducted a statistical analysis using the following methods:
  - (a) **Frequency Distribution of Pixel Distances:** The frequency distribution of pixel distances between adjacent circle centers in both rows and columns was calculated, along with the error distribution in image compared to the actual geometric distances.
  - (b) **Radius Error Analysis:** The frequency distribution of the detected circle radius was computed, and the error distribution was analyzed by comparing the detected values with the actual radius size, along

with the error distribution in image.

- (c) **Resolution Comparison:** The accuracy of the pixel-distance mapping system was analyzed by comparing results obtained using 2k and 4k image resolutions, while keeping the perspective transformation resolution constant. This analysis provides insights for subsequent system development.
- (d) **Abnormal Case Analysis:** For any anomalies observed during statistical analysis, the circular dots detection process was visualized and analyzed to identify the causes of these anomalies. The error distribution patterns were summarized to guide improvements in the system's accuracy.

The figures in 5.3.1 and 5.3.2 illustrate the results of the static evaluation under 2k and 4k resolution:

1. **Frequency Distribution of Euclidean Distances Between Adjacent Centers:** These frequency figures show the frequency distributions of Euclidean distances between adjacent circular dots within the same row and column, both in their raw form and after logarithmic normalization.
2. **2D Spatial Distribution of Distance Errors:** The spatial distribution of Euclidean distance errors is mapped in a two-dimensional space corresponding to the perspective transformation image, providing insight into error patterns.
3. **Frequency Distribution of Detected Dot Radius:** These frequency figures include the frequency distribution of the detected dot radius, both in their raw form and after logarithmic normalization, and the spatial distribution of radius errors in the perspective transformation image.
4. **Filtered Dot Pattern with Perspective Transformation:** These figures show the dot pattern extracted after perspective transformation and contour detection. The encoded row numbers (binary encoding, with red representing 1 and black representing 0) are identified for each dot. The green numbers on the left represent counters, indicating the cumulative number of rows detected in the image, while the red numbers on the right display the binary-encoded values of the dots.
5. **Outlier Identification and Annotation:** Using the frequency distributions and error distributions, the corresponding positions of outliers are identified and annotated in the perspective-transformed image. This facilitates further analysis to determine the causes of the errors.

The table in Section 5.3.3 provides a statistical analysis of the mean, variance, and median based on the figures presented in Sections 5.3.1 and 5.3.2. This

analysis is conducted to evaluate the accuracy of the pixel-distance mapping method and offers recommendations for future development and application.

### 5.3.1 Dots Based Evaluation in 2k Image Resolution

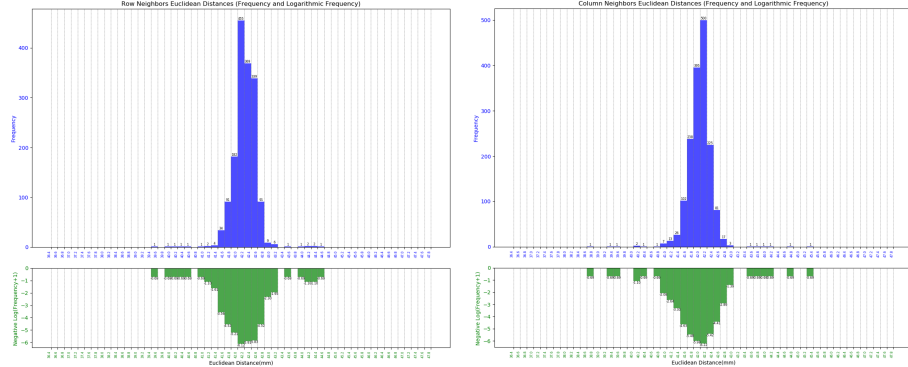


Figure 18: Frequency and Logarithmic Frequency of adjacent dot (row and column) Euclidean distances in camera 0 (2k)

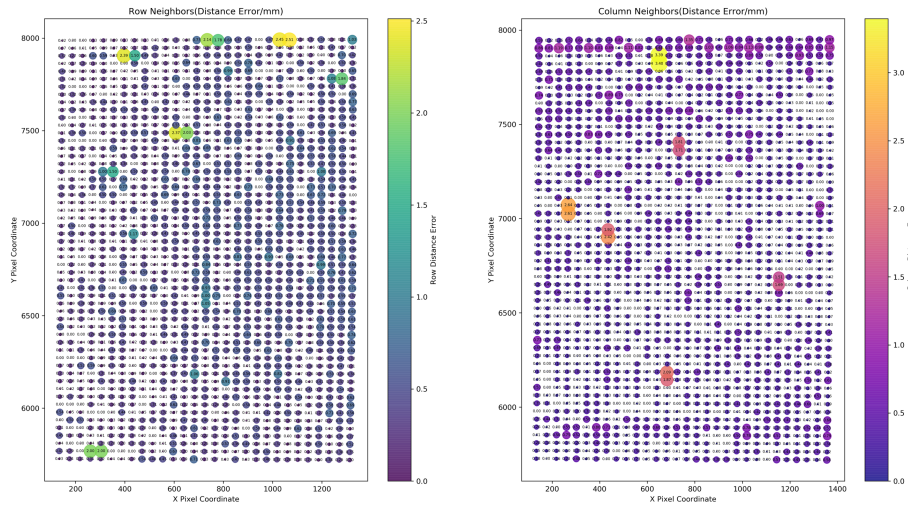


Figure 19: The distribution of adjacent dot (row and column) Euclidean distances error in camera 0 (2k)

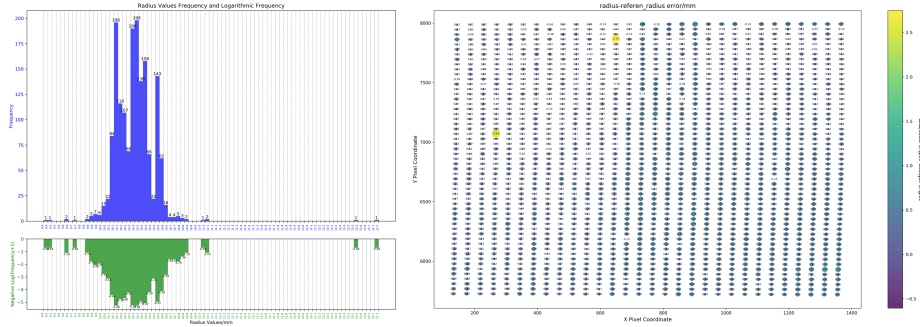


Figure 20: Frequency and Logarithmic Frequency of detected dot radius value and the distribution of radius error in camera 0 (2k)

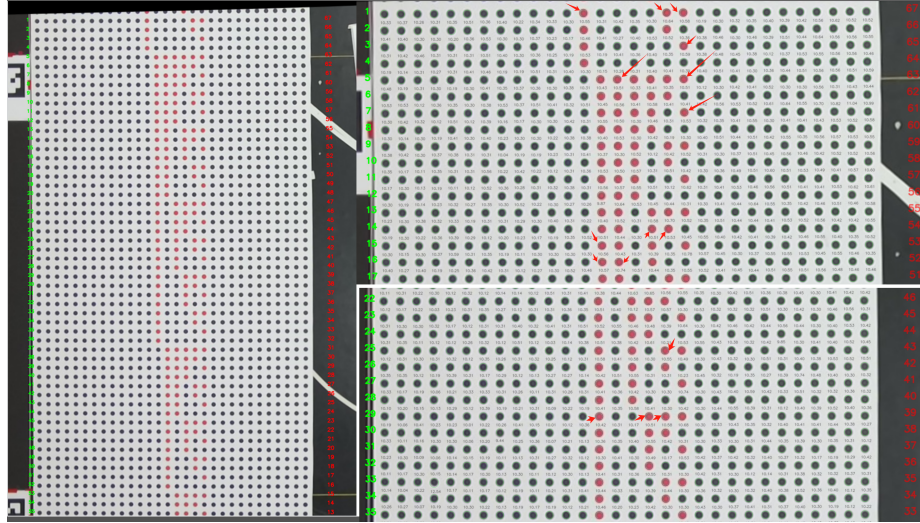


Figure 21: The detected dot in camera 0 (2k)

Figures 18-19 illustrate the frequency distribution of Euclidean distances between adjacent circle centers detected by camera0 at a 2k resolution. As shown in the figures, the Euclidean distances between adjacent circle centers range from 39.4 mm to 45.4 mm, with most distances concentrated in the range of 41.4 mm to 42.8 mm.

Figure 20 displays the spatial distribution of errors, where most errors are located along the upper edge of the image, while a few larger errors are scattered at different positions. Combining this with Figure 21, it can be observed that some of the scattered errors correspond to positions where red and black dots alternate.

Additionally, Figure 20 shows that the detected circle radius for camera0 at a 2k resolution range from 9.4 mm to 12.7 mm. A few outliers exhibit a significant difference from the actual radius size, with deviations ranging from 2.54 mm to 2.57 mm.

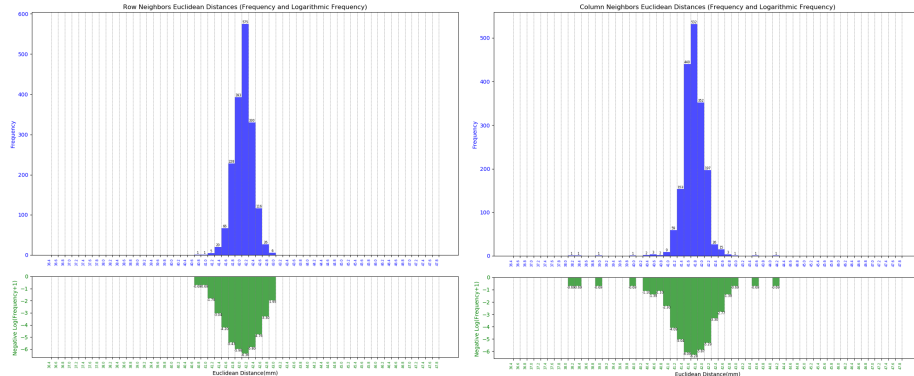


Figure 22: Frequency and Logarithmic Frequency of adjacent dot (row and column) Euclidean distances in camera 1 (2k)

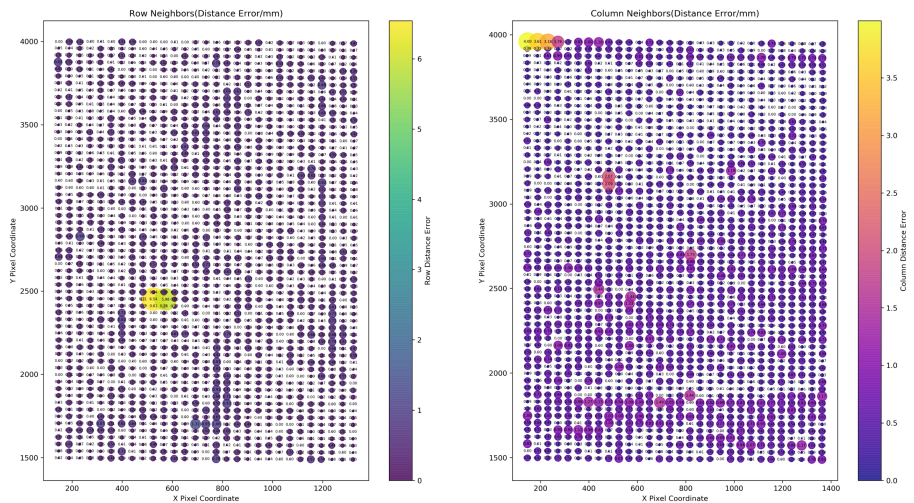


Figure 23: The distribution of adjacent dot (row and column) Euclidean distances error in camera 1 (2k)

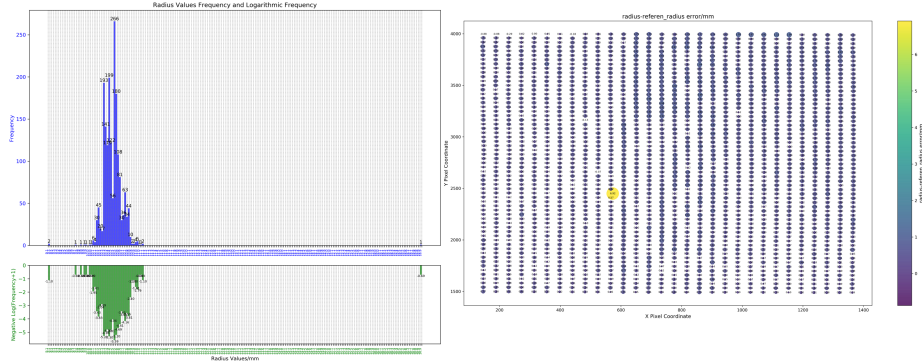


Figure 24: Frequency and Logarithmic Frequency of detected dot radius value and the distribution of radius error in camera 1 (2k)

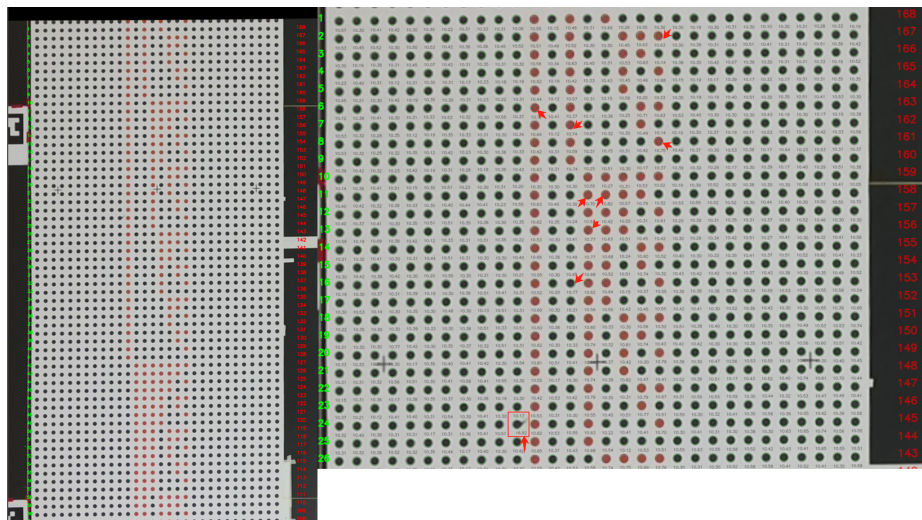


Figure 25: The detected dot in camera 1 (2k)

Figures 22-23 present the frequency distribution of Euclidean distances between adjacent circle centers detected by camera1 at a 2k resolution. The figures show that the distances range from 38.2 mm to 44.2 mm, with most distances concentrated in the range of 41.2 mm to 42.6 mm.

Figure 24 illustrates the spatial distribution of errors, where most errors are located in the upper-right corner of the image, while a few larger errors are scattered in various positions. Combined with Figure 26, it can be observed that some of these scattered errors correspond to positions where red and black dots alternate. Among the dots encoded as row 146, there is one dot with a

significantly larger detected radius and visible contamination.

Figure 25 shows the distribution of detected circle radius by camera1 at a 2k resolution, ranging from 9.2 mm to 16.92 mm. One outlier with an abnormally large radius corresponds to the contaminated dot in row 146 of the original image.

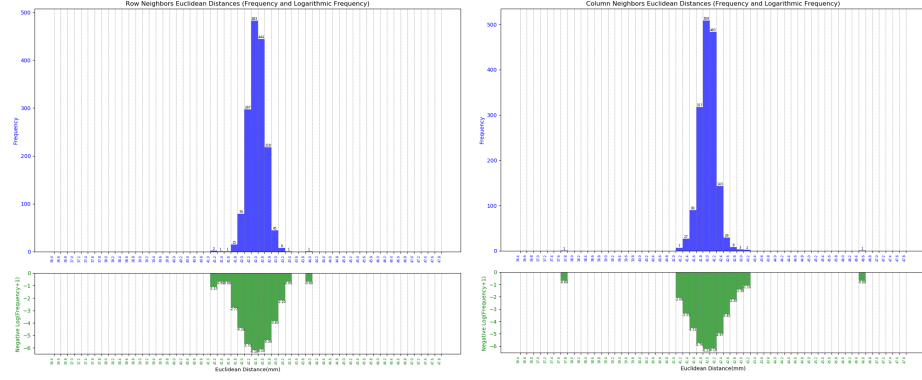


Figure 26: Frequency and Logarithmic Frequency of adjacent dot (row and column) Euclidean distances in camera 2 (2k)

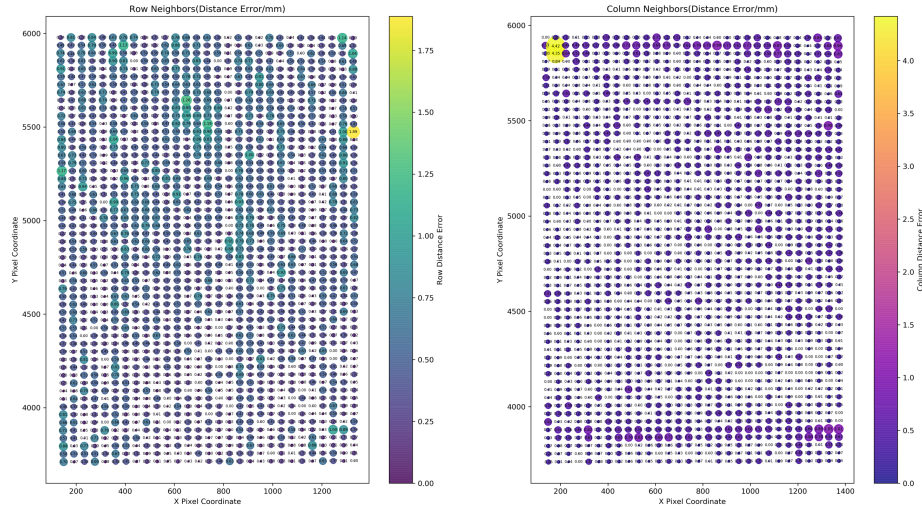


Figure 27: The distribution of adjacent dot (row and column) Euclidean distances error in camera 2 (2k)

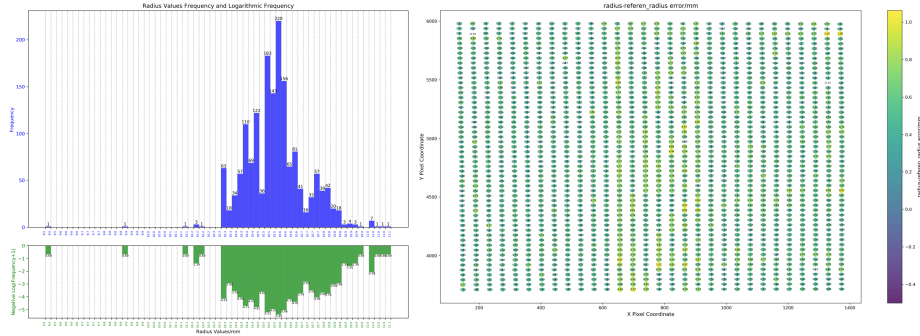


Figure 28: Frequency and Logarithmic Frequency of detected dot radius value and the distribution of radius error in camera 2 (2k)

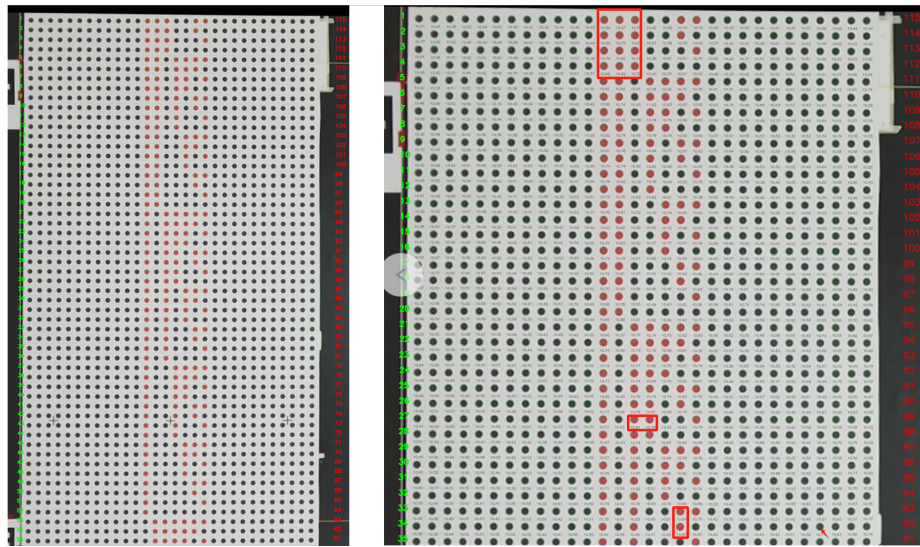


Figure 29: The detected dot in camera 2 (2k)

Figures 26-28 present the frequency distributions of Euclidean distances between adjacent circle centers, circle radius, and the error distribution detected by camera2 at a 2k resolution.

As shown in Figure 29, the radius of the red dots are generally slightly larger than those of the black dots. This difference leads to slightly larger distance discrepancies at positions where red and black dots alternate compared to other locations.

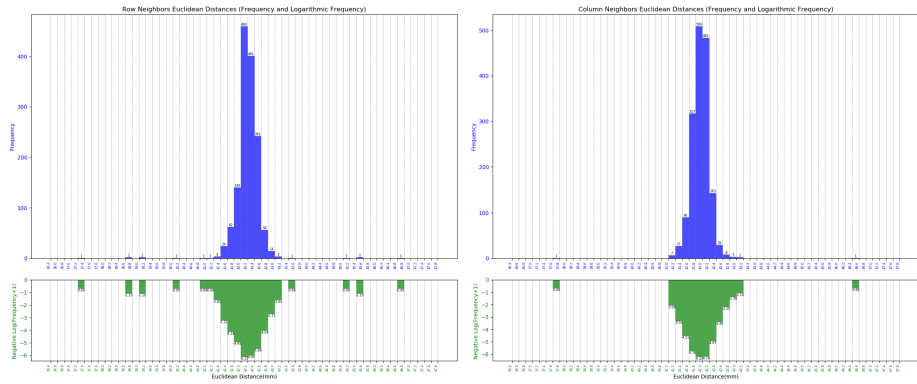


Figure 30: Frequency and Logarithmic Frequency of adjacent dot (row and column) Euclidean distances in camera 3 (2k)

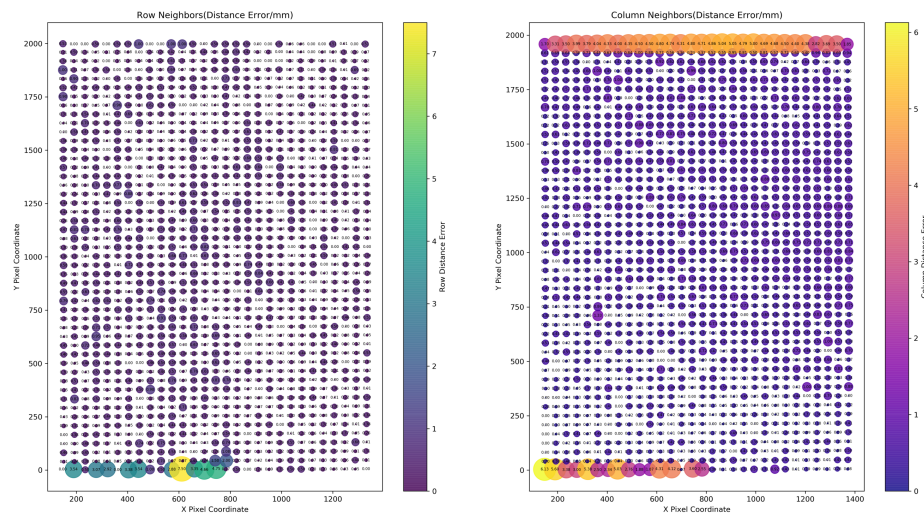


Figure 31: The distribution of adjacent dot (row and column) Euclidean distances error in camera 3 (2k)

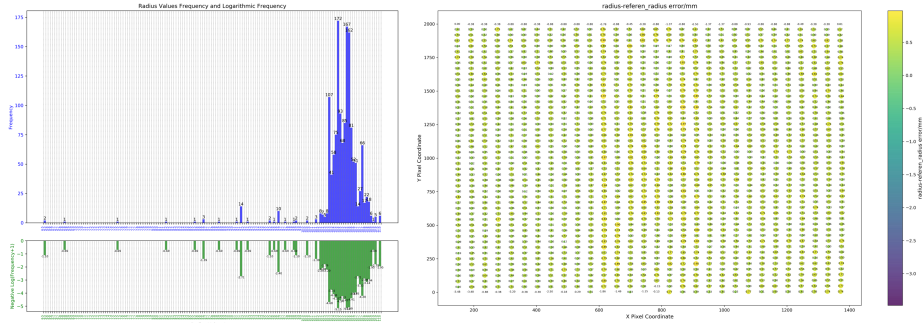


Figure 32: Frequency and Logarithmic Frequency of detected dot radius value and the distribution of radius error in camera 3 (2k)

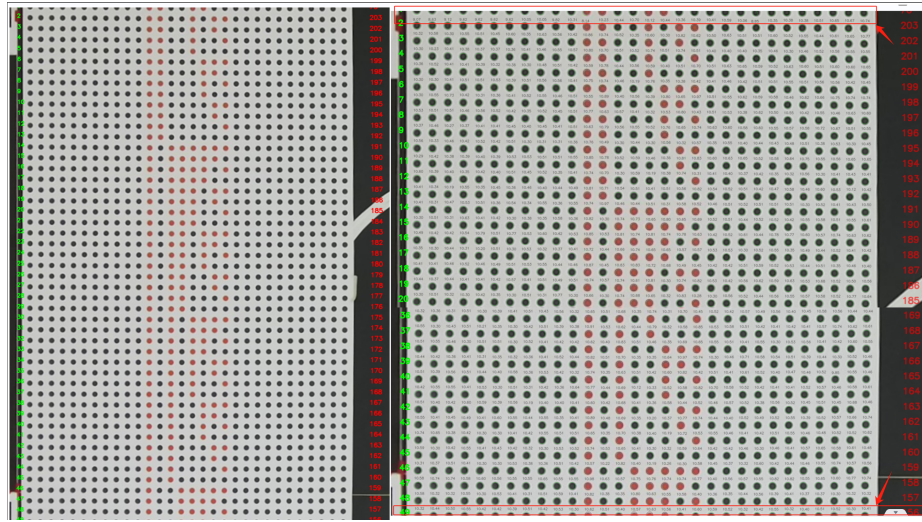


Figure 33: The detected dot in camera 3 (2k)

Figures 30-32 present the frequency distributions of Euclidean distances between adjacent circle centers, circle radius, and the error distribution detected by camera3 at a 2k resolution. The figures reveal that distance and radius errors are significantly larger along the upper and lower edges of the image, often appearing as entire rows with consistently large errors or exhibiting patterns of gradual increase or decrease.

As shown in Figure 33, this phenomenon occurs because incomplete circles along the upper and lower edges of the image are being detected. This results in predicted circle center positions and radius that deviate significantly from their actual values.

### 5.3.2 Dots Based Evaluation in 4k Image Resolution

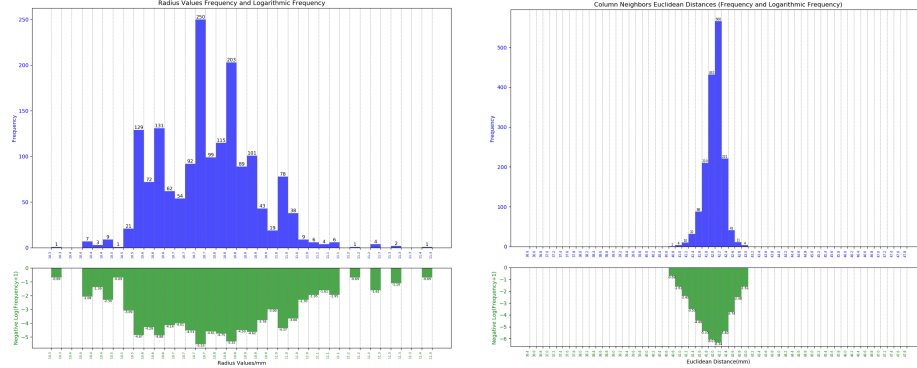


Figure 34: Frequency and Logarithmic Frequency of adjacent dot(row and column) Euclidean distances in camera 0 (4k)

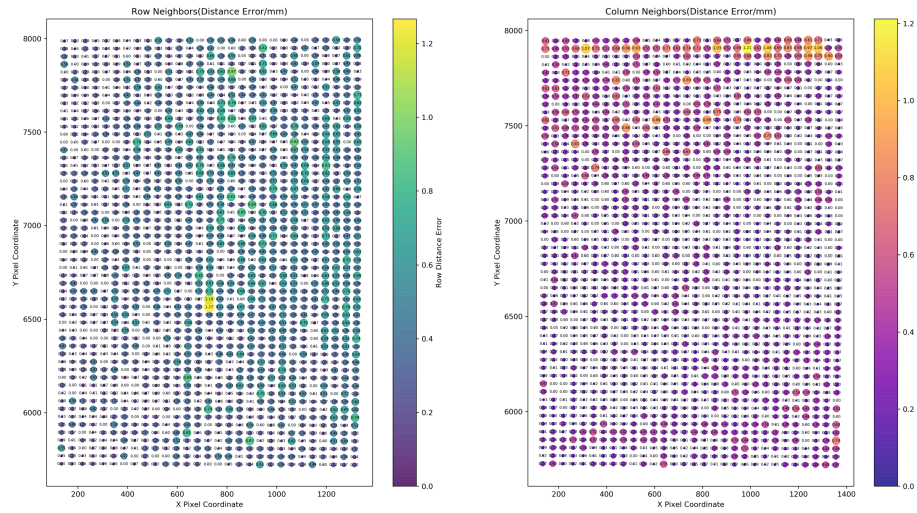


Figure 35: The distribution of adjacent dot (row and column) Euclidean distances error in camera 0 (4k)

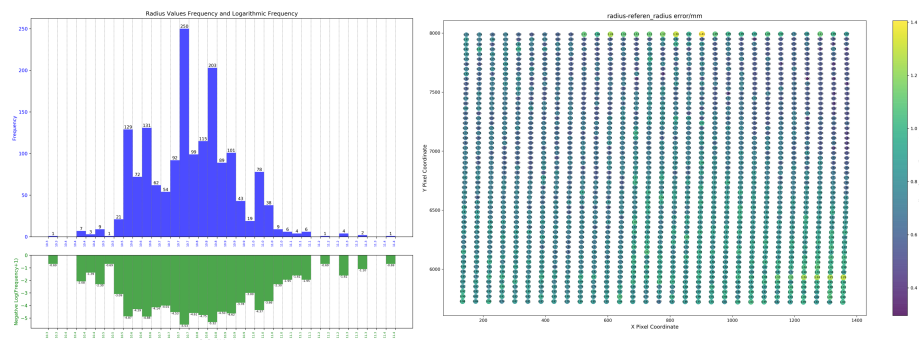


Figure 36: Frequency and Logarithmic Frequency of detected dot radius value and the distribution of radius error in camera 0 (4k)

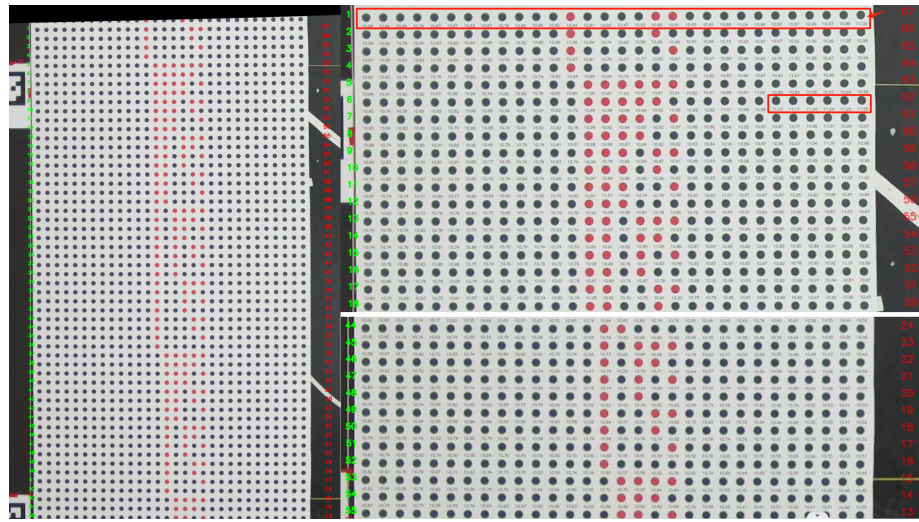


Figure 37: The detected dot in camera 0 (4k)

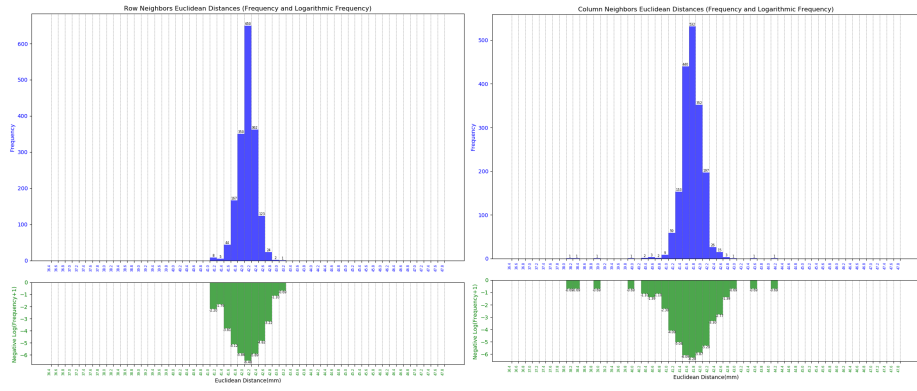


Figure 38: Frequency and Logarithmic Frequency of adjacent dot (row and column) Euclidean distances in camera 1 (4k)

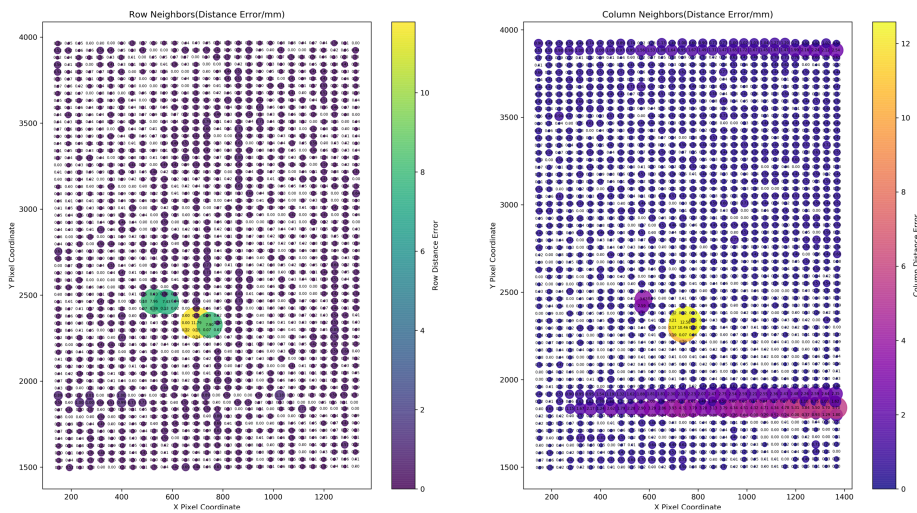


Figure 39: The distribution of adjacent dot (row and column) Euclidean distances error in camera 1 (4k)

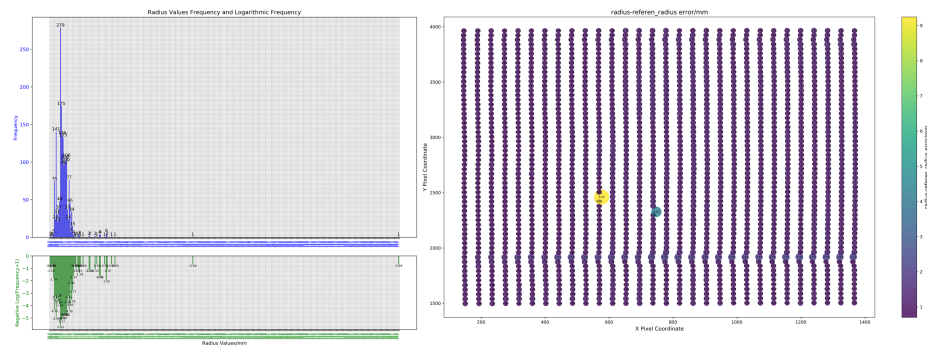


Figure 40: Frequency and Logarithmic Frequency of detected dot radius value and the distribution of radius error in camera 1 (4k)

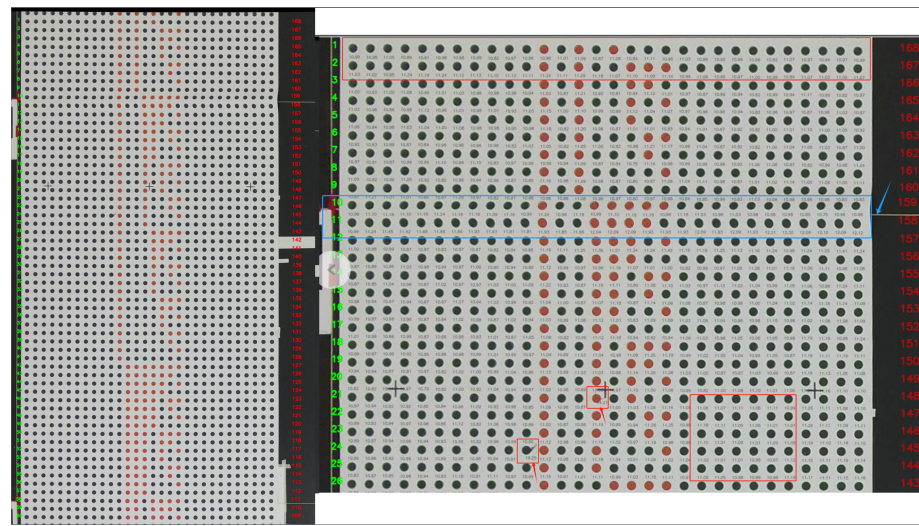


Figure 41: The detected dot in camera 1 (4k)

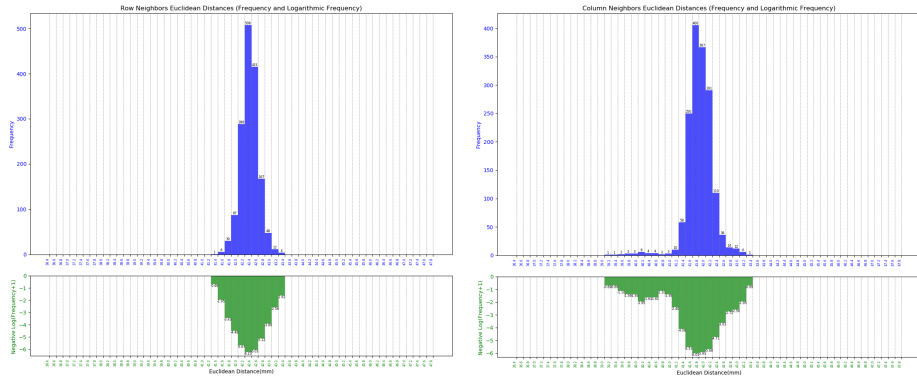


Figure 42: Frequency and Logarithmic Frequency of adjacent dot (row and column) Euclidean distances in camera 2 (4k)

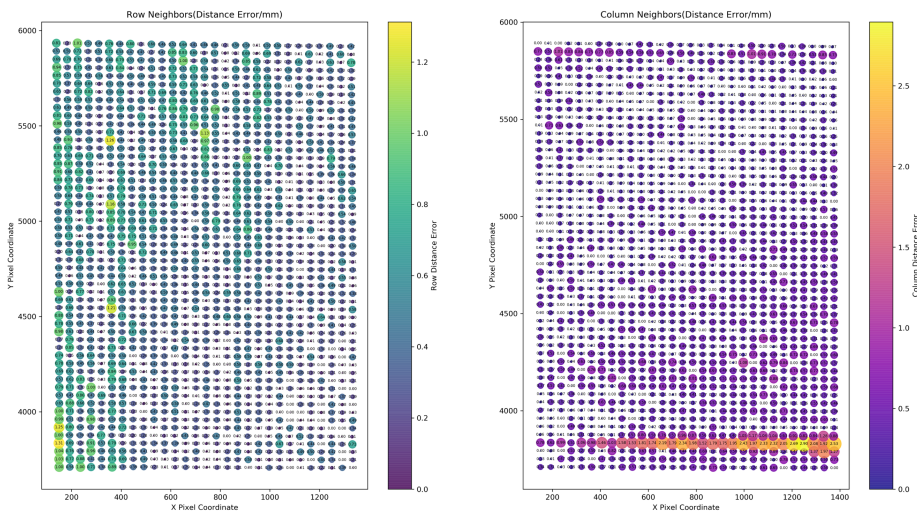


Figure 43: The distribution of adjacent dot (row and column) Euclidean distances error in camera 2 (4k)

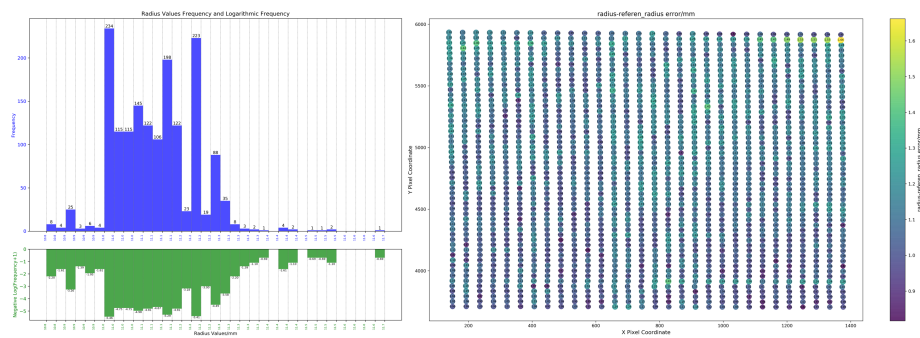


Figure 44: Frequency and Logarithmic Frequency of detected dot radius value and the distribution of radius error in camera 2 (4k)

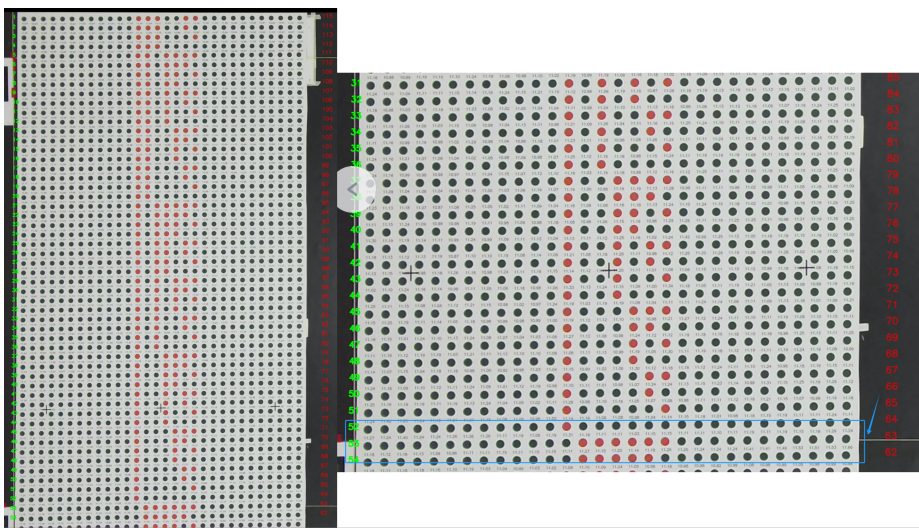


Figure 45: The detected dot in camera 2 (4k)

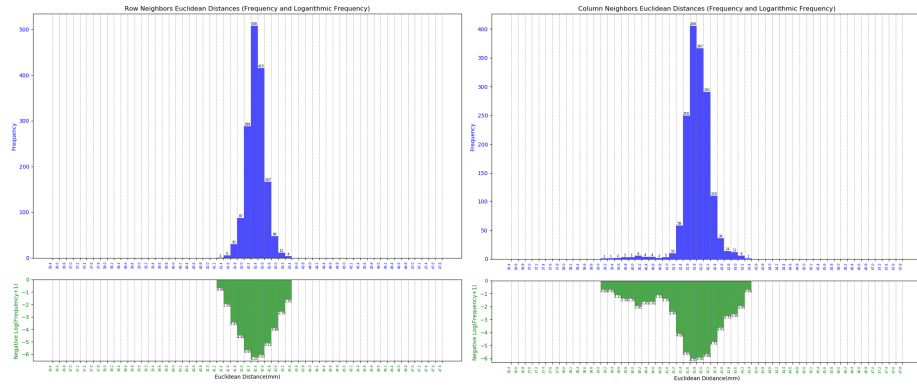


Figure 46: Frequency and Logarithmic Frequency of adjacent dot (row and column) Euclidean distances in camera 3 (4k)

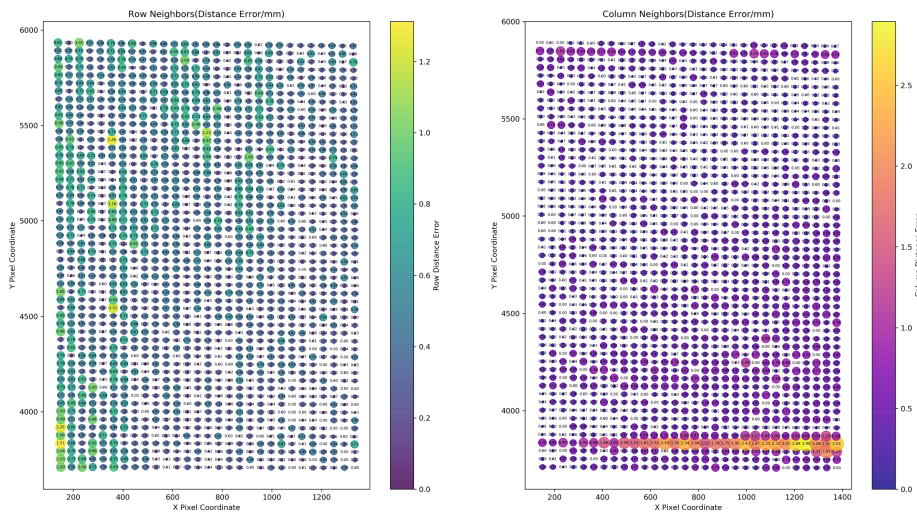


Figure 47: The distribution of adjacent dot (row and column) Euclidean distances error in camera 3 (4k)

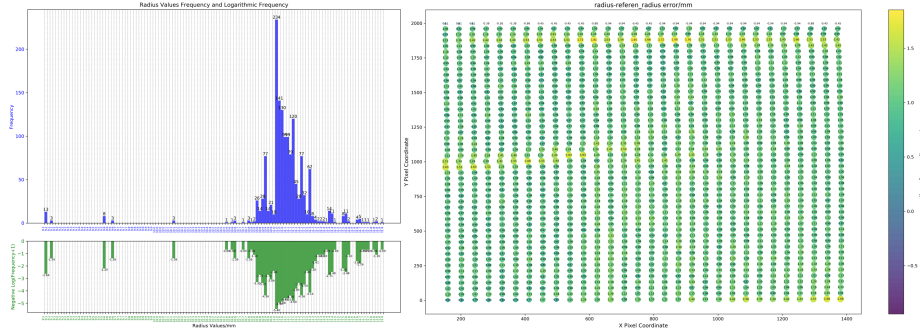


Figure 48: Frequency and Logarithmic Frequency of detected dot radius value and the distribution of radius error in camera 3 (4k)

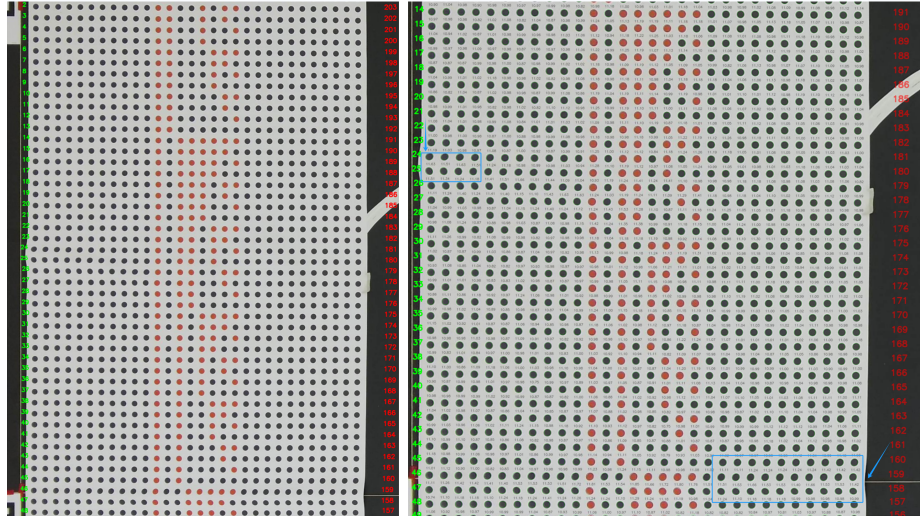


Figure 49: The detected dot in camera 3 (4k)

Figures 34-44 illustrate the frequency distributions of Euclidean distances between adjacent circle centers, circle radius, and the error distributions detected by the four cameras at a 4k resolution. In cameras 1, 2, and 3, there are one or two consecutive rows in non-edge regions with significantly larger distance and radius errors. Analysis reveals that this is caused by the physical reference lines overlapping with the dot pattern, resulting in slight protrusions in the canvas at these positions. These protrusions affect the detection of circle contours as well as the estimation of circle positions and radius.

At these locations, the circles exhibit noticeable deformations in the 4k resolution images, which are less visible in the 2k resolution images. Notably,

the radius error of the contaminated dot in row 146 of camera1 is significantly larger at 4k resolution compared to 2k resolution. Overall, except for camera1, the Euclidean distances and circle radius detected by the other three cameras demonstrate relatively concentrated frequency distributions.

### 5.3.3 Error Analysis and Prospects in Dots Based Evaluation

#### Error analysis

Camera Id	Mean (mm)	Median (mm)	Variance (mm)
0	42.20	42.21	0.1137
1	42.04	42.03	0.1180
2	42.36	42.37	0.0641
3	42.20	42.20	0.1954
mean	42.20	42.20	0.1228

Table 4: Statistical results of Euclidean distances between adjacent detected dots in rows in 2k.

Camera Id	Mean (mm)	Median (mm)	Variance (mm)
0	42.20	42.21	0.0796
1	42.07	42.06	0.2433
2	42.34	42.33	0.0683
3	42.20	42.20	0.0945
mean	42.20	42.20	0.1214

Table 5: Statistical results of Euclidean distances between adjacent detected dots in rows in 4k.

Camera Id	Mean (mm)	Median (mm)	Variance (mm)
0	41.97	42.00	0.1218
1	41.68	41.69	0.1036
2	41.93	41.93	0.0821
3	41.55	41.62	0.5028
3	41.55	41.62	0.5028
mean	41.78	41.81	0.2026

Table 6: Statistical results of Euclidean distances between adjacent detected dots in column in 2k.

<b>Camera Id</b>	<b>Mean (mm)</b>	<b>Median (mm)</b>	<b>Variance (mm)</b>
0	41.97	42.00	0.0689
1	41.78	41.79	0.5531
2	41.82	41.82	0.1486
3	41.52	41.63	0.6605

Table 7: Statistical results of Euclidean distances between adjacent detected dots in column in 4k.

<b>Camera Id</b>	<b>Mean (mm)</b>	<b>Median (mm)</b>	<b>Variance (mm)</b>
0	10.30	10.31	0.0348
1	10.46	10.46	0.0524
2	10.54	10.53	0.1486
3	10.46	10.51	0.0995

Table 8: Statistical results of detected dots radius value in 2k.

<b>Camera Id</b>	<b>Mean (mm)</b>	<b>Median (mm)</b>	<b>Variance (mm)</b>
0	10.75	10.74	0.0186
1	11.04	11.01	0.5531
2	11.09	11.09	0.0095
3	11.02	11.03	0.0818

Table 9: Statistical results of detected dots radius value in 4k.

Tables 4-9 provide a comparative analysis of the mean, variance, and median values for the Euclidean distances between adjacent circle centers and the circle radius detected by the four cameras at 2k and 4k resolutions.

At both 2k and 4k resolutions, the mean and median values of row-wise distances are approximately 42 mm, with errors fluctuating within 0.4 mm. Similarly, the column-wise distances have slightly smaller mean and median values than 42 mm, with errors fluctuating within 0.5 mm. The differing error averages for row and column distances may be attributed to camera distortion. From the perspective-transformed images, distortion is more noticeable in the upper regions of the images, with camera0 and camera1 showing slightly more distortion and camera3 showing less. Although distortion correction was applied during processing, some residual distortion correction errors may remain.

Tables 8-9 indicate that the detected circle radius at 2k resolution are approximately 10 mm, with errors fluctuating within 0.55 mm, while at 4k resolution, the radius are around 11 mm, with errors fluctuating within 1.1 mm. The 4k resolution may amplify errors introduced by distortion correction and perspective

transformation, while also allowing more fine-grained details to be captured. As seen in the perspective-transformed images in Sections 5.3.1 and 5.3.2, the 4k resolution reveals deformations caused by the uneven dot canvas plane due to the added reference strings. This observation aligns with the actual conditions, whereas such deformations are not visually discernible at 2k resolution and are also undetectable in the corresponding error distribution maps.

Apart from the dot canvas in the field of view of camera1, which includes a row with a visible contamination mark, both 2k and 4k resolutions detected the contaminated circle. However, the contour-based calculation yielded a circle center position and radius larger than the actual values. The radius error at 4k resolution is significantly larger than at 2k, indicating that the higher resolution may also magnify such errors. This contributes to the larger variance of radius errors for camera1 at 4k compared to 2k. In contrast, for the other three cameras, the variance of both distance and radius errors at 4k resolution is smaller than at 2k, demonstrating that the contours of circles detected at 4k resolution are more stable and accurate.

### Prospects in Dots Based Evaluation

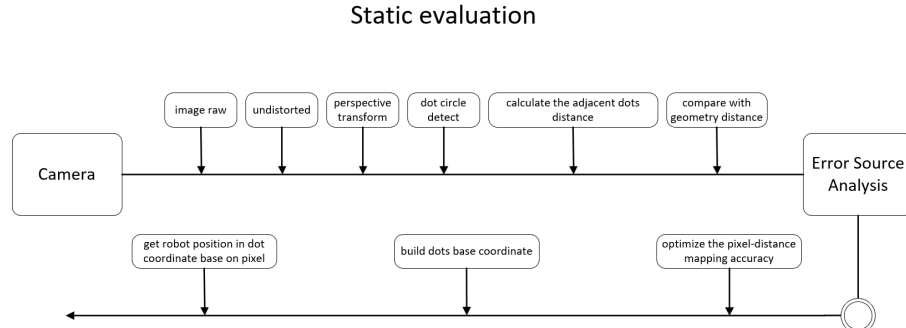


Figure 50: Future works of dots based evaluation

The above analysis and comparison of 2k and 4k resolutions are based on the same perspective transformation resolution. For higher-resolution 4k images, it is possible to adopt a higher pixel-distance mapping scale. Once the pixel-distance mapping achieves a certain level of precision (while also accounting for the effect of height on pixel-distance mapping, which was not considered in the evaluations of Section 5.3), the detected dot pattern can be used to establish a coordinate system. This coordinate system could serve as a foundation for robot navigation.